**Proceedings of the ASME 2010 10th Biennial Conference on Engineering Systems Design and Analysis**
**ESDA2010**
**July 12-14, 2010, Istanbul, Turkey**

**25436**

# EXPERIMENTS ON THE NONLINEAR DYNAMICS OF PARALLEL PLATES SUBJECTED TO SQUEEZE-FILM FORCES

**Philippe Piteau**
Commissariat à l'Energie Atomique
Laboratoire d'Études de Dynamique
CEA/DEN/DM2S/SEMT/DYN
Saclay, France

**José Antunes**
Instituto Tecnologico e Nuclear
Applied Dynamics Laboratory
ITN/ADL
Sacavem, Portugal

## ABSTRACT

Squeeze film dynamical effects are relevant in many industrial components, bearings and seals being the most conspicuous applications. But they also arise in other industrial contexts, for instance when dealing with the seismic excitation of spent fuel racks. The significant nonlinearity of the squeeze-film forces prevents the use of linearised flow models, therefore a fully nonlinear formulation must be used for adequate computational predictions. Because it can accommodate laminar and turbulence flow effects, a simplified bulk-flow model – based on gap-averaged Navier-Stokes equations and incorporating all relevant inertial and dissipative terms – was previously developed by the authors (Antunes & Piteau, 2010), assuming a constant skin-friction coefficient. In this paper we introduce an improved theoretical formulation, fully developed elsewhere (Piteau & Antunes, 2010), such that the dependence of the friction coefficient on the local flow velocity is explicitly accounted for, so that it can be applied to laminar, turbulent and mixed flows. The main part of the paper is then devoted to the presentation and discussion of the results from an extensive series of experiments performed at CEA/Saclay. The test rig consisted on a long gravity-driven instrumented plate of rectangular shape colliding with a planar surface. Theoretical results stemming from both analytical flow models are confronted with the experimental measurements, in order to assert the strengths and drawbacks of the simpler original model, as well as the improvements brought by the new but more involved flow formulation.

## INTRODUCTION

Many systems of practical interest are subjected to intense fluid/structure interaction forces when a thin layer of fluid is interposed between two vibrating structures. A typical example is provided by immersed structural components, which may impact if an external excitation is imposed. Nonlinear effects can then become dominant and should not be neglected. Significant work in this field has been performed at CEA/Saclay during the last two decades, in connection with nuclear facilities – see Esmonde et al. (1990a,b) and Antunes & Piteau (2001,2010).

The extensive literature on the fluid/structure dynamics of industrial squeeze-film problems is mostly concerned with linearised analysis, the vibratory motions being such that, at each location $\mathbf{r}$, the fluctuating part $\tilde{h}(\mathbf{r},t)$ of the local fluid gap $h(\mathbf{r},t)=\bar{h}(\mathbf{r})+\tilde{h}(\mathbf{r},t)$ is small compared to the mean gap value $\bar{h}(\mathbf{r})$ – see, for instance, works by Fritz (1970), Hobson (1982), Mulcahy (1980,1988) and Moreira et al. (2000a), as well as the review books by Païdoussis (1998) and Kaneko et al. (2008). One of the most thorough analysis along these lines was achieved by Inada & Hayama (1990a,b), under steady flow, who evaluated the fluidelastic force under steady flow, including added mass, damping and stiffness flow terms for a one-dimensional tapered leakage channel. More recently, Porcher & DeLangre (1997) evaluated the dynamical effects of changing the loss coefficients at the channel inlet and outlet boundary conditions.

The linearised approach is obviously unable to provide answers at larger vibratory amplitudes, when the fluctuating gap $\tilde{h}(\mathbf{r},t)$ is of the same order of magnitude as $\bar{h}(\mathbf{r})$. Finding a suitable analytical formulation for the fully nonlinear problem is the main subject of the present paper. Here we will address the case of squeeze-film dynamics under no permanent flow, which in a sense restricts our previous efforts in this field, see Antunes & Piteau (2001,2010). However, our previous dynamical solution will be now extended in order to encapsulate, in the analytical formulation of the nonlinear fluid coupling force, the flow velocity dependence of the dissipative terms. Overall, the analytical formulation developed here may be connected with our approach in work focused on immersed rotor dynamics – see Axisa & Antunes (1992), Grunenwald (1994), Antunes et al. (1996), Antunes et al. (1999), Moreira et al. (2000a,b). Actually, the successful "bulk-flow" approach started by Fritz (1970) and Hirs (1973), and later used by many authors – see Childs (1993) – appears also well suited to deal with small-to-moderate fluctuating gaps, such as found in the configuration of the problems addressed here.

We start by recalling our nonlinear flow model obtained by assuming constant (velocity independent) flow friction coefficients, see Antunes & Piteau (2001,2010). Apart from the specific dissipative terms connected with our quadratic-in-velocity pressure drop formulation, we obtain fluid forces which are similar to those previously presented by Esmonde et al. (1990a). Then we refine our formulation in order to incorporate the dependence on flow velocity of the loss coefficients, which are conveniently expressed in terms of a single formulation, suitable for laminar or turbulent conditions, as well as mixed flows. We thus produce a unique analytical solution for the coupling fluid force applied to the plates, irrespectively of the nature of the flow inside the gap. Such improved model is only briefly sketched here, as it is thoroughly reported by Piteau and Antunes (2010) elsewhere.

The second and main part of this paper relates to experimental results performed at CEA/Saclay, on the motion of a gravity-driven plate colliding with a rigid plane surface. This example is motivated by impact problems which may arise between immersed nuclear components, such as fuel racks. The colliding plate has dimensions such that the width $W$ is much larger than the length $L$, therefore the flow may be assumed approximately one-dimensional, along the shorter dimension $L$. Extensive experiments have been performed, in particular by changing the fluid temperature, hence its viscosity. These experimental results are reported and compared with both the basic and refined models of the fluid force, with general satisfying agreement. Furthermore, the strengths and drawbacks of the older model are discussed, and the improvements brought by the new but more involved flow formulation are highlighted.

## THEORETICAL FLOW MODEL

The bulk-flow continuity and momentum equations for 1D incompressible flows within small-to-moderate fluctuating gaps are well established – see, for instance, Childs (1993), Antunes et al. (1996) or Antunes & Piteau (2010):

$$\frac{\partial h}{\partial t} + \frac{\partial}{\partial x}\left(hu\right) = 0 \tag{1}$$

$$\rho\left[\frac{\partial}{\partial t}\left(hu\right) + \frac{\partial}{\partial x}\left(hu^2\right)\right] = -\left(\tau_1^x + \tau_2^x + h\frac{\partial p}{\partial x}\right) \tag{2}$$

Furthermore, we will assume in this paper that the plate surfaces are parallel – see Figure 1 – so that $h(x,t) = Y(t)$, $\forall x$, where for simplicity it will be assumed that the lower plate is fixed and the fluid gap $Y(t)$ is given by the displacement of the upper plate.

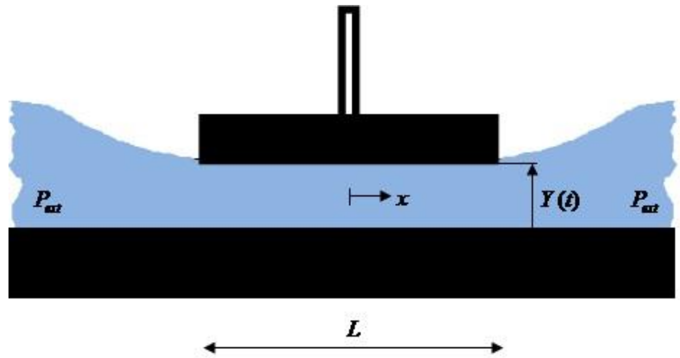


**Figure 1: Geometry of the fluid-structure system analysed, with moving parallel plates coupled to an incompressible fluid.**

The dynamic force exerted by the fluid per unit width of the plate – e.g., the total force is $W\,F_f(t)$ – is given by:

$$F_f(t) = \int_{-L/2}^{L/2} p(x,t)\,dx = 2\int_0^{L/2} p(x,t)\,dx \tag{3}$$

where the last form is justified by the problem symmetry, which enables working on the positive half-space region only.

Following the bulk-flow approach, the tangential stresses $\tau_1^x$ and $\tau_2^x$ will be formulated using a loss-of-head model:

$$\tau_{1,2}^x = \frac{1}{2}\rho u\left|u\right| f_{1,2} \tag{4}$$

where the friction coefficients at the walls $f_1$ and $f_2$ are established based on empirical correlations – see Idel'Cik (1960) and Blevins (1984). Typically, $f$ changes with the flow Reynolds number as (Hirs, 1973):

$$f = n\left(\text{Re}\right)^m \quad \text{with} \quad \text{Re}(x,t) = \frac{2h(x,t)\left|u(x,t)\right|}{\nu} \tag{5}$$

where parameters $m$ and $n$ depend on the flow. For *turbulent flows* between plane smooth surfaces, Hirs suggest the following values:

$$10^3 < \text{Re} < 3\,10^4 \;\Rightarrow\; m_T = -0.25 \;\;,\;\; n_T = 0.055 \tag{6}$$

On the other hand, for *laminar flows*, the friction coefficient decreases very fast for increasing flow velocities. In rectangular channel it can be easily shown that:

$$\text{Re} < 4\,10^3 \;\Rightarrow\; m_L = -1 \;\;,\;\; n_L = 12 \tag{7}$$

Beyond these distributed stresses, other singular dissipative effects arise in the boundaries $x = \pm L/2$ of the moving plate. Very complex phenomena arise here and, in the absence of reliable and extensive loss data obtained from unsteady flow configurations, we will adopt – as in many other investigations – a classic quasi-static Bernoulli formulation with a loss term at the channel/reservoir interfaces. Hence, at $x = \pm L/2$:

$$p\left(\pm L/2,t\right)+1/2\,\rho\left[u\left(\pm L/2,t\right)\right]^2 = \\ = P_{ext} \pm 1/2\,\rho u\left(\pm L/2,t\right)\left|u\left(\pm L/2,t\right)\right| K_{in,out}\left[\mathrm{Re}\left(\pm L/2,t\right)\right] \quad (8)$$

where $P_{ext}$ is a static reference pressure in an external reservoir, far from the singularity, and the loss coefficients $K_{in,\,out}$ depend on the local geometry and Reynolds number. Idel'Cik (1960) and Blevins (1984) give extensive values for the singular loss coefficient $K_{in,out}(\mathrm{Re})$, as a function of the flow direction (entering or leaving the channel), of the Reynolds number and of the channel/reservoir interface geometry. For turbulent flows and an abrupt gap change, typical values are $K_{in} \approx 0.5$ (when $\dot{Y}(t) > 0$) and $K_{out} \approx 1$ (when $\dot{Y}(t) < 0$). In general, smooth (rounded) corners of the plates at $x = \pm L/2$ will lead to lower values of $K_{in}$. On the other hand, low velocity flows will lead to increased values of the loss coefficient.

Concerning *distributed losses*, notice that the dichotomy of the formulation for the friction coefficients – equation (5) with either parameters (6) or (7) – creates a difficulty with using the bulk-flow formulation: Turbulent regimes lead to tangential stresses which depend almost quadratically on the average flow velocity, through a friction coefficient $f_T$ which is almost independent of the flow velocity. On the other hand, because the laminar tangential stresses increase proportionally to the flow velocity, then for consistence the quadratic formulation (4) implies a laminar friction coefficient decreasing in $f_L \sim \mathcal{O}(1/u)$. In general terms, from equations (4) to (7), we may write for *turbulent flows*:

$$\tau^{(T)}_{1,2} = \frac{1}{2}\rho u|u| n_T \left(\frac{2h|u|}{\nu}\right)^{m_T} = \frac{2^{m_T-1} n_T \rho}{\nu^{m_T}} h^{m_T} u|u|^{m_T+1} \quad ; \quad \mathrm{Re} > \mathrm{Re}_0 \quad (9)$$

and for *laminar flows*:

$$\tau^{(L)}_{1,2} = \frac{1}{2}\rho u|u| n_L \left(\frac{2h|u|}{\nu}\right)^{m_L} = \frac{2^{m_L-1} n_L \rho}{\nu^{m_L}} h^{m_L} u|u|^{m_L+1} \quad ; \quad \mathrm{Re} < \mathrm{Re}_0 \quad (10)$$

where $\mathrm{Re}_0$ is the Reynolds number separating the laminar and turbulent flow ranges.

For any realistic values of the constants $n_L$, $m_L$, $n_T$ and $m_T$, it is clear that $\tau^{(T)}_{1,2}/\tau^{(L)}_{1,2}$ is negligible in the range $\mathrm{Re} < \mathrm{Re}_0$, while $\tau^{(L)}_{1,2}/\tau^{(T)}_{1,2}$ can be neglected in the range $\mathrm{Re} > \mathrm{Re}_0$. Then, a very simple and natural choice for a continuous function emulating the behavior of (6) and (7) in the *full range* of laminar and turbulent flows is:

$$\tau_{1,2} = \frac{1}{2}\rho u|u| n_L \left(2h|u|/\nu\right)^{m_L} + \frac{1}{2}\rho u|u| n_T \left(2h|u|/\nu\right)^{m_T} \\ = C_L \rho h^{m_L} u|u|^{m_L+1} + C_T \rho h^{m_T} u|u|^{m_T+1} \quad ; \quad \forall\,\mathrm{Re} \quad (11)$$

with constants:

$$C_L = 2^{m_L-1} n_L / \nu^{m_L} \quad ; \quad C_T = 2^{m_T-1} n_T / \nu^{m_T} \quad (12)$$

Figure 2 displays the result of approximating the Hirs friction model using formulation (11), which highlights the adequacy of the approach adopted.

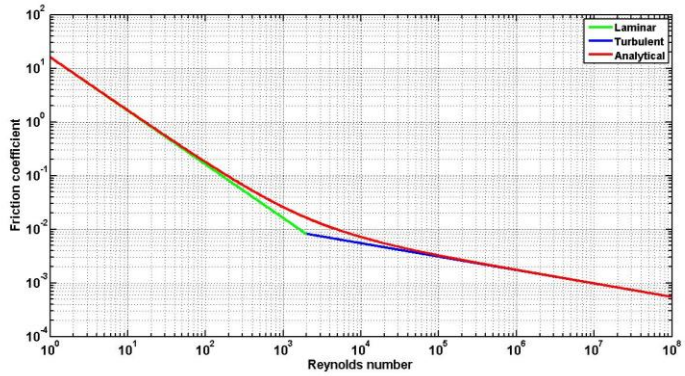


**Figure 2: Comparison between the Hirs friction model (5)-(7) with the continuous analytical approximation (11)-(12).**

We now turn to the *singular loss coefficients* at the channel boundaries, which change in a more drastic manner according to the direction of the flow (either entering or being ejected from the channel), on the boundary geometry (abrupt or smooth change of fluid gap), on the nature of the flow (laminar or turbulent), as well as on the Reynolds number. Idel'Cik (1960) and Blevins (1984) provide guidelines for a number of standard geometries, as a function of the Reynolds number, following given assumptions on the flow velocity profiles. For any actual nonlinear time-domain computation, it is easy to compute $K_{in,out}\left[\mathrm{Re}\left(L/2,t\right)\right]$ by interpolating through the published experimental values. Unfortunately, our tested geometry does not conform exactly to any of the cases detailed in these references. Therefore, we decided to use in our numerical simulations a constant value for the singular loss coefficient, which both fits our experimental data and is generally consistent with these references.

## DYNAMICAL FLOW FORCE

Here, the external static pressure on reservoir at the left side of the plate is equal to the static pressure on the right side, $P_{ext}$. For our basic formulation, we postulate that the skin-friction coefficients are independent of the flow velocity and that the plate surfaces are similar, so that $f_1 = f_2 \equiv f \;\; (\forall\,\mathrm{Re})$. From equations (1) to (4), we obtain the following explicit form for the total dynamic force of the fluid on the plates, per unit width:

$$F_f(t) = P_{ext} L - \frac{\rho L^3}{12}\frac{\ddot{Y}}{Y} + \frac{\rho L^3}{24}\frac{\dot{Y}^2}{Y^2} - \frac{\rho L^4}{32}\frac{\dot{Y}|\dot{Y}|}{Y^3} f - \frac{\rho L^3}{8}\frac{\dot{Y}|\dot{Y}|}{Y^2} K_{in,out}\left[\mathrm{Re}\left(L/2,t\right)\right] \quad (13)$$

where one can recognize, beyond the trivial constant force term stemming from $P_{ext}$, four vibration-induced nonlinear dynamical terms which are related to: (a) the local fluid inertia, (b) the convective inertia, (c) the distributed wall interface stresses, and (d) the singular losses at the boundaries. Notice that the magnitude of all these force terms increase dramatically as the fluid gap closes, because of the various powers of $Y(t)$ in the denominators of (13) – hence the squeeze-film effect.

Note that, as discussed before, in the previous integration the friction coefficient $f$ was assumed constant, which is not actually true. For turbulent flows the exponent $m$ is quite small, so that the change of the friction coefficient with flow velocity becomes second order and the preceding simplification is justified. However, if the flow velocity is low enough, laminar flows will arise and the convenient simplification leading to solution (13) will entrain some error. Such is the case for the geometry of Figure 1, as symmetry imposes that near the middle of the plate $u(0,t)=0$, therefore a (smaller or larger) region of the channel will *always* display laminar flow, whatever the values of $Y(t)$ and $\dot{Y}(t)$ which may well lead to turbulent flows in the outer regions of the channel.

Most terms in solution (13) are analogous to those published by Esmonde et al. (1990a). However, our quadratic dissipative term related to flow/wall stresses is different from theirs, due to the distinct assumptions involved. Both coefficients $K_{in}$ and $K_{out}$ can be used when performing a numerical simulation, the first one during aspiration ($\dot{Y}(t)>0$) and the other during ejection ($\dot{Y}(t)<0$).

The new and more general solution, which applies to mixed laminar/turbulent flows, is obtained from (1)-(3) with the Reynolds-dependent skin-friction stresses modeled according to (11)-(12). We obtain the following dynamic force of the fluid on the plates, per unit width – see Piteau & Antunes (2010):

$$F_f(t)=P_{ext}L-\frac{\rho L^3}{12}\frac{\ddot{Y}}{Y}+\frac{\rho L^3}{24}\frac{\dot{Y}^2}{Y^2}-\frac{2^{m_L-2}C_L\rho L^{m_L+4}}{m_L+4}\frac{\dot{Y}\left|\dot{Y}\right|^{m_L+1}}{Y^3}-$$
$$-\frac{2^{m_T-2}C_T\rho L^{m_T+4}}{m_T+4}\frac{\dot{Y}\left|\dot{Y}\right|^{m_T+1}}{Y^3}-\frac{1}{8}\rho L^3\frac{\dot{Y}\left|\dot{Y}\right|}{Y^2}K_{in,out}\left[\mathrm{Re}\left(L/2,t\right)\right] \quad (14)$$

Finally, for the single degree of freedom system shown in Figure 1, we have the equation for coupled flow/structure dynamics:

$$M_s\ddot{Y}(t)+C_s\dot{Y}(t)+K_s\left[Y(t)-H\right]=W\,F_f\left(Y(t),\dot{Y}(t),\ddot{Y}(t)\right)+F_e(t) \quad (15)$$

with the fluid force given by either (13) or (14) and $F_e(t)$ is any given externally applied force. On the other hand, $H$ is the reference value of the fluid gap, for the non-excited system. This is time-step integrated using any adequate algorithm. We used an explicit Runge-Kutta method, with variable time-step controlled by an estimate of the local integration error. For the experimental system tested, we have $K_s=0$ and $F_e(t)=M_s g$.

## EXPERIMENTAL VALIDATION

The experimental set-up, shown in Figure 3, consists on an immersed rectangular plate with dimension $L\times W=55\times 214$ mm, which is dropped from an height $Y_0=15$ mm. The plate is free to move along the vertical direction, when subjected to gravity, so that $K_s=0$, the total mass of the mobile fixture being $M_s=36.6$ Kg. However, there is some damping $C_s=200$ Ns/m in a plate-guiding device. The fluid is water, with volumic mass $\rho=1000$ Kg/m$^3$ and kinematic viscosity $\nu=10^{-6}$ m$^2$/s at normal temperature. However, several tests were also performed at other temperatures, in order to change the viscosity (and hence the Reynolds number), as discussed in the following.

The fluid force was measured using two force piezo-transducers Kistler 9117AB (with charge amplifiers Kistler 5011), mounted symmetrically between the plate and the sustaining fixture, at locations $x=\pm 95$ mm. The plate motion was sensed using a non-contact displacement transducer Kaman KD2300-6C, mounted along the vertical direction, providing a linear response in the range $Y=0\sim 6$ mm. Furthermore, two acceleration transducers Endevco 224C (with charge amplifiers B&K 2635) where used, one of them being processed with an analogue integrator, in order to obtain the velocity response of the plate.

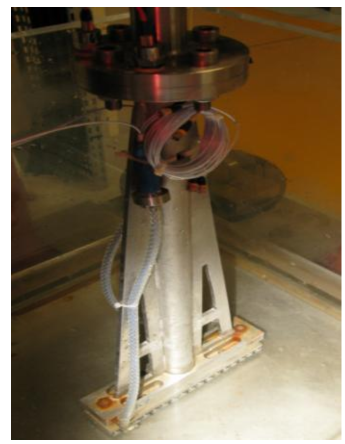

**Figure 3: General view of the experimental rig and detail of the rigid instrumented plate.**

As a preliminary verification of the plate/base parallelism, we show in Figure 4 a sample response of the left and right force transducers, stemming from a typical drop test. It can be seen that the traces are almost indistinguishable, confirming a near-perfect symmetrical distribution of the dynamical fluid pressure, hence a satisfying parallel geometry of the experimental fluid gap. Notice however that, after the large force spike related to the fluid force $F_f(t)$, some other complex phenomenon arises. This secondary feature in the experimental responses is not related to fluid forces, but to a solid contact between the plate ant the base arising at the very end of the drop motion, which leads to a plate rebound. Such behavior, which was consistently observed, is a direct and unavoidable consequence of any residual lack of planarity of the plate and base surfaces, which ultimately becomes dominant as $Y(t) \to 0$. Our theoretical model obviously does not apply to such phenomenon, which we did not try to emulate.

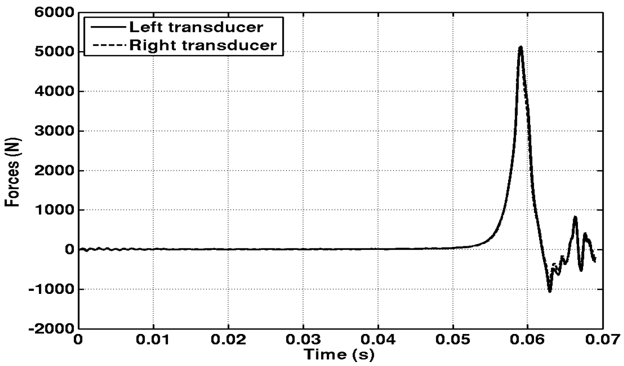


**Figure 4: Sample measured forces by the two plate transducers, demonstrating the parallelism of the plate/base assembling.**

The width-to-length ratio $W/L = 3.9$ of the tested plate is quite significant. Nevertheless, it may not be sufficient to rule-out an experimental "error" connected with the 2D flow component under the plate squeezing, which is not addressed in our theoretical formulations. Even so, the 1D flow models addressed here will be confronted with these experimental results, on the reasonable ground that such 2D effect should be of second order magnitude.

In Figure 5 we compare the experimental results of a plate drop at temperature 20ºC with the theoretical predictions stemming from our general model (14) for mixed laminar/turbulent flow. Here, the theoretical results were obtained using parameters (6), pertaining to Hirs empirical correlation for distributed skin-friction stresses. On the other hand, as mentioned earlier, our experimental geometry does not conform exactly to any of the geometries for which the inlet/outlet singular loss coefficients are tabulated in reference works – see Idel'Cik (1960) and Blevins (1984). Therefore some incertitude exists concerning the value(s) of $K_{out}$ which apply to our experiments – note that in these tests the fluid is always ejected (at least before rebounding occurs), so only the outlet coefficient is relevant. After some numerical testing, we tentatively opted for a straightforward engineering approach, which proves effective. Actually, we use in our numerical simulations a constant value for $K_{out}$ which both fits well our experimental data and is generally consistent with the referenced values. For all tests, the value $K_{out} = 0.85$ fulfilled both conditions.

Notice that the experimental displacement signal in Figure 5 is saturated when $Y(t) > 6$ mm, because the beginning of the motion lays beyond the transducer range. Also notice the complex motion which arises at the end of the motion, because of spurious solid contact, as discussed before. In general, the motion of the dropping plate and the dynamical fluid force are well predicted by the theoretical model, except for the acceleration at near-contact.

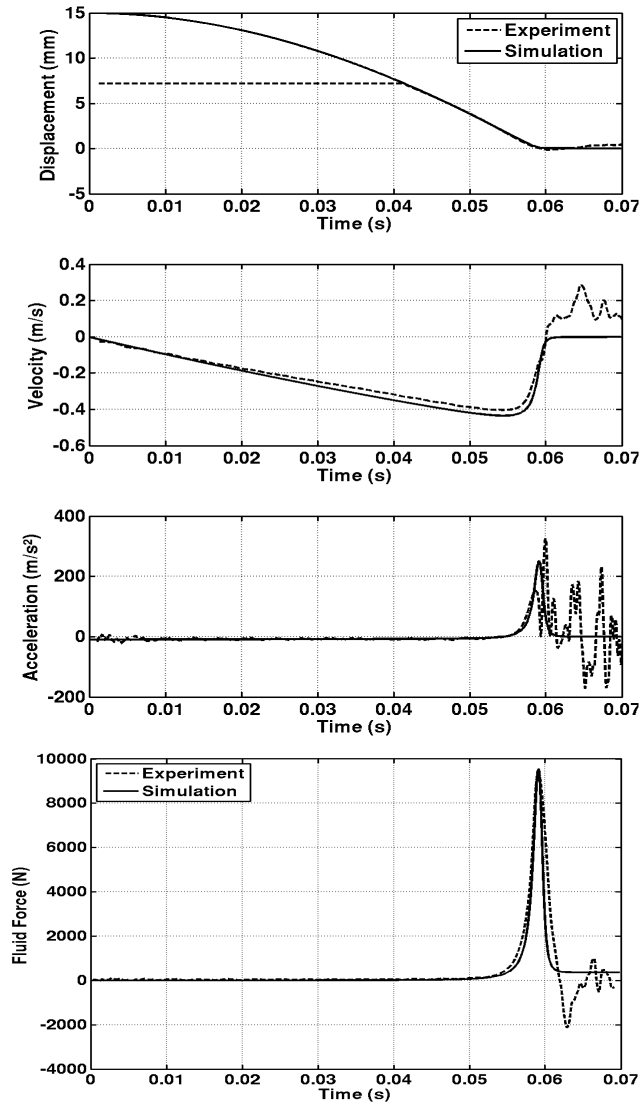


**Figure 5: Comparison of the experimental plate motion (displacement, velocity and acceleration) and dynamical fluid force with the theoretical solution from the general formulation with Hirs empirical correlation encapsulated, using a singular loss coefficient $K_{out} = 0.85$ (drop test at temperature 20ºC).**

For future comparison, it will prove interesting to plot illustrative time-histories of the Reynolds number (5) and of the corresponding variable friction coefficient, as computed from Hirs formulation. These are plotted in Figure 6, at two locations along the channel ($x = 0.25\,L/2$ and $x = 0.75\,L/2$), for the computation results shown in Figure 5. Notice that, as expected from the velocity field computed from (1), $u(x,t) = -x\dot{Y}/Y$, the Reynolds number increases when approaching the plate boundary. Also note that, during most of the time, the friction coefficient approaches $f \approx 0.01$, although a two-decade increase is experienced at the beginning and near the end of the motion.

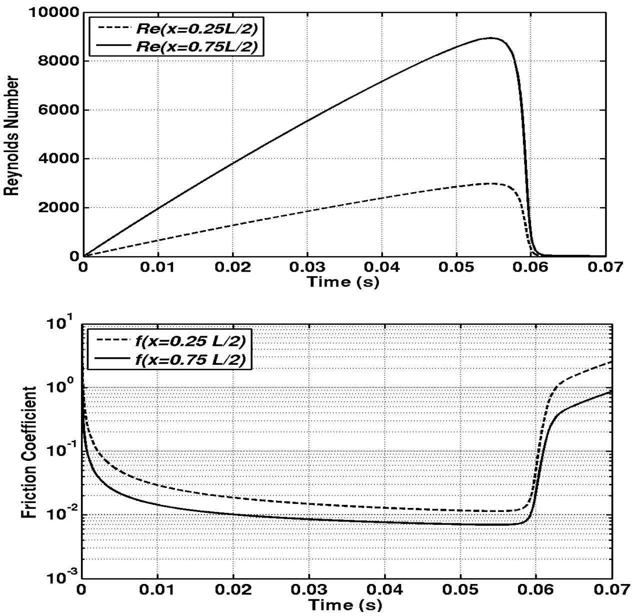


**Figure 6: Time-histories of the Reynolds number and of the corresponding friction coefficient, computed from the general formulation with Hirs correlation $f(\mathrm{Re})$, at two different locations along the channel (all parameters as in Figure 5).**

We now turn to the theoretical predictions from the simplified model (13), with constant friction coefficient. The fluid forces predicted are shown by the plots in Figure 7, respectively for constant friction values of $f = 0.01$ and $0.1$ (and using, as before, $K_{out} = 0.85$), which from the results of Figure 6 might be reasonable guesses. Actually, the results obtained when using $f = 0.01$ are quite usable, however those stemming from $f = 0.1$ clearly underestimate the fluid force. One can thus conclude that the simplified model (13) may well produce good predictions, provided an adequate value of the "constant" friction coefficient is supplied. However, by incorporating the velocity dependence $f(\mathrm{Re})$, our new improved analytical solution eliminates incertitude and guesswork concerning this parameter. At the cost of a modest increase in the model complexity, we believe that the gains from the refined solution far surpass this slight drawback.

Figure 8 shows the time-histories of the Reynolds numbers, corresponding to the computations of Figure 7. Notice that these Reynolds numbers are quite insensitive to the actual value of the friction coefficient. Actually, both results are also quite similar to the plot connected with the variable friction coefficient, shown in Figure 6. This suggests that, for this fluid/structure coupled system, the flow pressure field is more sensitive to friction effects than the velocity field.

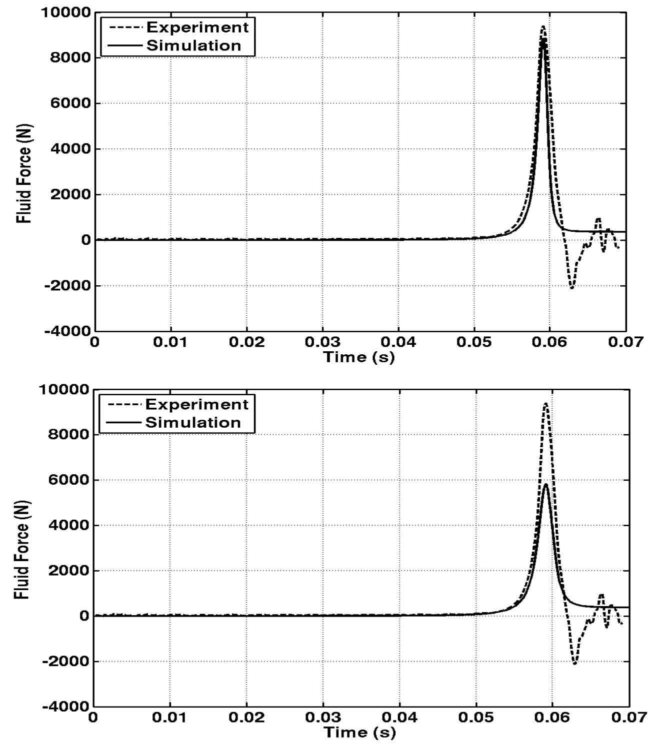


**Figure 7: Comparison of the experimental dynamical fluid force with theoretical solutions from the simplified model with constant friction coefficient, for values $f = 0.01$ (upper plot) and $f = 0.1$ (lower plot), and using the singular loss coefficient $K_{out} = 0.85$ (drop test at temperature 20ºC).**

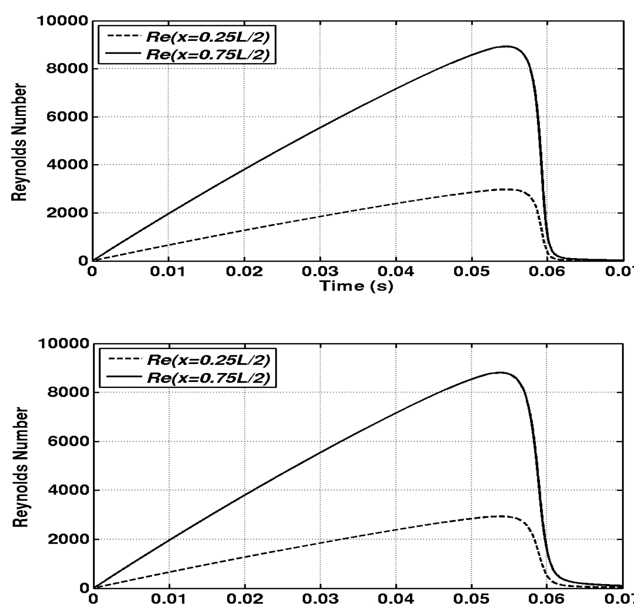


**Figure 8: Time-histories of the Reynolds number, computed from the simplified model with constant friction coefficients $f = 0.01$ (upper plot) and $f = 0.1$ (lower plot), at two different locations along the channel (all parameters as in Figure 7).**

 

In Figures 9 and 10 we have decomposed the total fluid force, to highlight the various inertia (local and convective) and dissipative (distributed and singular losses) terms, as per equations. Figure 9 pertains to the computation results shown in Figure 5, with velocity-dependent friction coefficient, from the general model (14). The plots in Figure 10 pertain to the computations shown in Figure 7, with constant friction coefficient, from the simplified model (13).

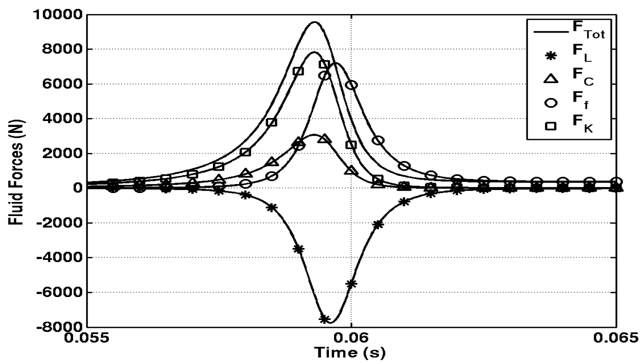


**Figure 9: Decomposition of the dynamical fluid force into inertia and dissipative terms, from the improved theoretical model with Reynolds-dependent friction coefficient (all parameters as in Figure 5).**

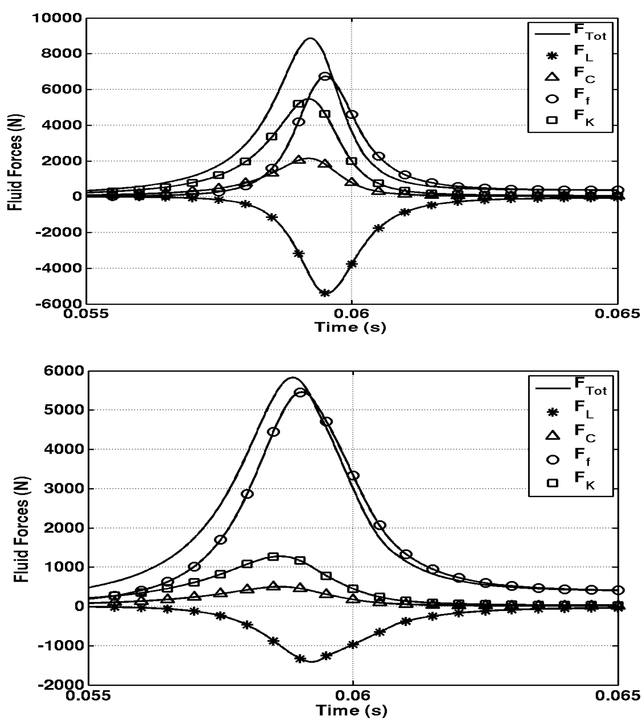


**Figure 10: Decomposition of the dynamical fluid force into inertia and dissipative terms, from the simplified model with constant friction coefficients, respectively for $f = 0.01$ (upper plot) and $f = 0.1$ (lower plot) (all parameters as in Figure 7).**

In Figure 9 the dissipative terms display similar magnitudes, although at different phases of the motion. Both have the same order of magnitude of the local inertia term, which is for this system the only term with opposite sign. The convective inertia term is the least significant of all. In Figure 10, the terms of the upper plot ( $f = 0.01$ ) follow similar trends, although with some quantitative differences. Not unexpectedly, the lower plot ( $f = 0.1$ ) is dominated by the skin-friction force term.

Our last results concern the influence of the fluid viscosity on the plate dynamics. Experiments were performed at four different temperatures, as shown in Table 1. Notice that the corresponding changes in viscosity enable a significant range of Reynolds numbers.

**Table 1: Physical data for the tests at several temperatures**

| Fluid temperature [ºC] | Volumic mass [Kg/m$^2$] | Kinematic viscosity [m$^2$/s] | Maximum Reynolds ( $x = \pm L/2$ ) |
|---|---|---|---|
| 2 | 1000 | 1.6 $10^{-6}$ | $\approx$ 7000 |
| 20 | 998 | 1.0 $10^{-6}$ | $\approx$12000 |
| 59.5 | 983 | 4.7 $10^{-7}$ | $\approx$25000 |
| 72 | 977 | 4.0 $10^{-7}$ | $\approx$30000 |

Figure 11 presents the experimental results obtained. Notice that the plots of the four test results are shown superimposed. The near-insensitivity of the system dynamics to the fluid temperature is striking. Furthermore, such behavior is also displayed by the theoretical results shown in Figure 12, where the plots shown were computed from the improved model with velocity-dependence of the friction coefficient, equation (14). This interesting behavior is better understood by looking at the force decompositions for two extreme temperatures, as shown in Figure 13. Notice that, in spite of the total forces being near-identical, there are significant differences in the various force terms – in particular the loss terms – which somehow self-compensate, leading to the same net result. In other words, if less energy is dissipated through the skin-friction term (because of a higher Reynolds number), then such "excess" energy leads to enhancing of other terms, which tend to compensate the difference.

## CONCLUSIONS

We have proposed in this paper a nonlinear analytical solution for the squeeze-film dynamical forces between parallel plates. Our approach is based on a 1D classical bulk-flow formulation and accommodates any kind of flow conditions along the channel gap, either laminar, turbulent or mixed flows. The time-domain computations presented show that a simpler formulation, using a constant skin-friction coefficient, may be able to produce satisfying predictions, provided a "good" average value of the friction coefficient is used. Nevertheless, because the improved formulation takes into account the space-time variation of $f\left[\mathrm{Re}(x,t)\right]$, it eliminates all guesswork concerning the friction stresses along the fluid channel. This considerable advantage comes at the modest cost of a slight increase in the complexity of the improved flow solution.

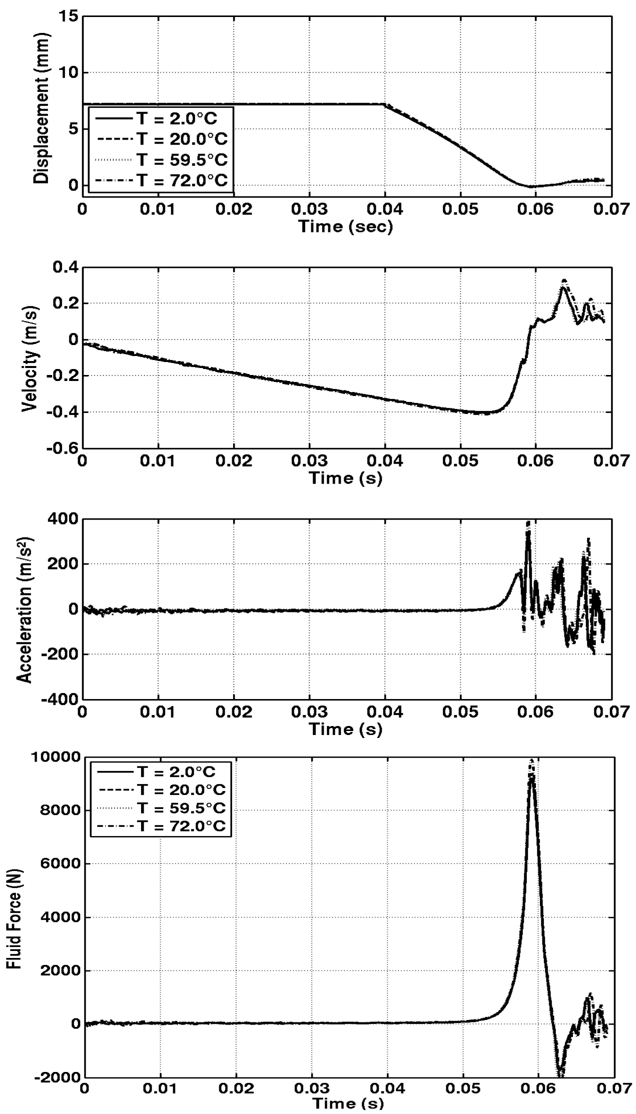


**Figure 11: Effect of the fluid temperature: Experimental plate motions (displacement, velocity and acceleration) and dynamical fluid forces.**

Computations performed on an immersed dropping plate show that all inertia and dissipative terms in the fluid force solution can be of significant magnitude. However the maximum amplitude of each term usually occurs at a different stage of the motion. For the specific system addressed, the distributed and singular friction losses lead to fluid force terms of similar magnitude. On the other hand, the least significant force term is related to the convective inertia. Analysis of the Reynolds number along the fluid channel indicates that, as expected, the flow is laminar near the centre of the moving plate but most often quite turbulent near the plate boundary. On the other hand, for the system studied in this paper, large increases in the velocity-dependent friction coefficient are experienced in the beginning as well as at the end of the plate drop motion. All these features stress the practical usability of the new improved flow force solution.

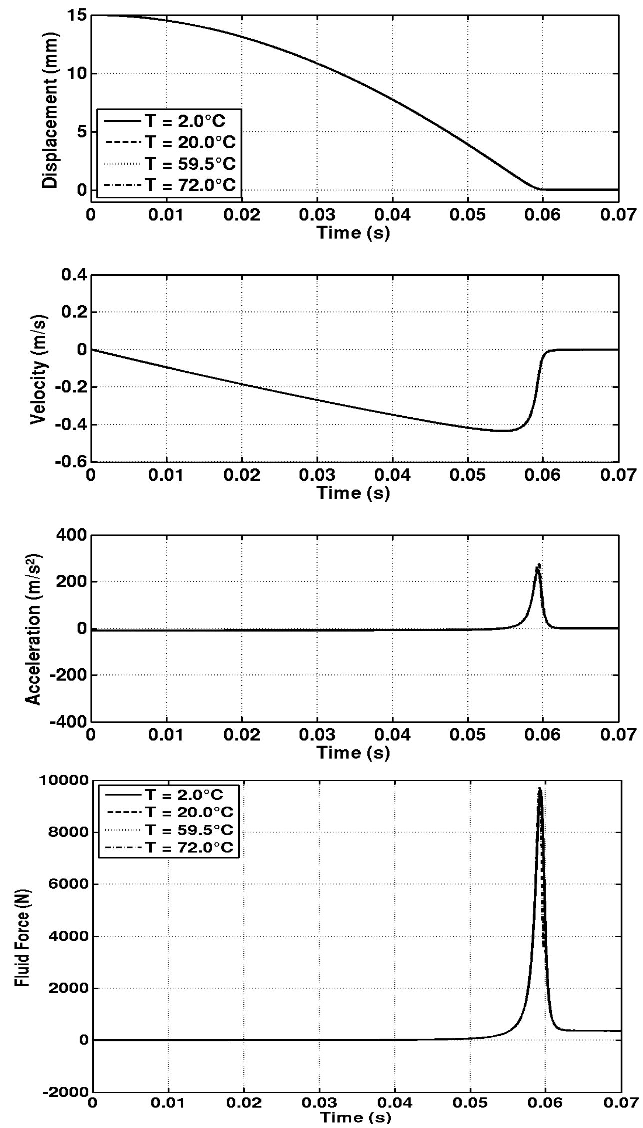


**Figure 12: Effect of the fluid temperature: Theoretical plate motions and dynamical fluid forces, computed from the general formulation with Hirs correlation $f(\mathrm{Re})$ and the singular loss coefficient $K_{out} = 0.85$.**

In the second part of this paper we presented and discussed the results of an extensive series of experiments performed at CEA/Saclay. These consisted on a long gravity-driven instrumented plate of rectangular shape colliding with a planar surface. Among the experimental results obtained, we presented a series of tests performed at various fluid temperatures, leading to a significant range of the flow Reynolds number. Interestingly, we consistently observed in both our experiments and computations that – although the various fluid force terms display some sensitivity to the actual Reynolds number along the squeeze-film channel – a kind of self-compensation actually arises between the various force terms, leading to a net fluid force which is nearly the same, irrespectively of the fluid viscosity.

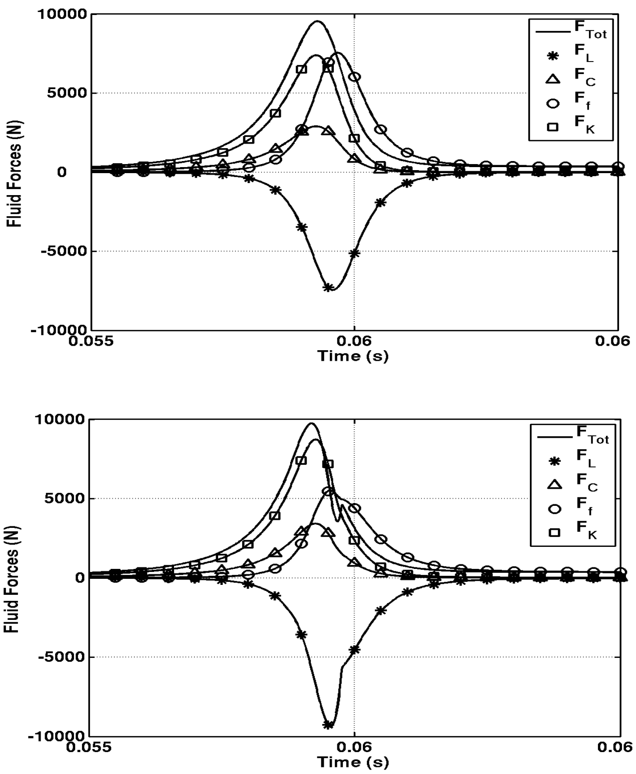


**Figure 13: Effect of the fluid temperature: Decomposition of the dynamical fluid force into inertia and dissipative terms, from the improved theoretical model with velocity-dependent friction coefficient, respectively for $T = 2°C$ (upper plot) and $T = 72°C$ (lower plot) (all parameters as in Figure 12).**

In all cases, our theoretical predictions were confronted with the experimental measurements with satisfying agreement. Nevertheless, one should keep in mind that some incertitude exists on the value of the singular loss coefficient which should be applied to our system. Here, we pragmatically overcame this problem by using a constant value for $K_{out}$ which both fits well our experimental results, while being generally consistent with the published data. Even if such approach produced quite acceptable results, further effort is needed to refine the manner in which this force term should be dealt. In a broader sense, modeling of the flow dissipative terms will certainly be improved when reliable loss coefficients for unsteady flows become available.

## ACKNOWLEDGMENTS

Concerning the experimental part of this work, we gladly acknowledge the valuable contribution of THIERRY VALIN, from CEA/DEN/DM2S/SEMT (Saclay, France).

## REFERENCES

Antunes, J., Axisa, F., Grunenwald, T. (1996), “Dynamics of Rotors Immersed in Eccentric Annular Flows: Part 1 - Theory”, Journal of Fluids and Structures, Vol. 10, pp. 893-918.

Antunes, J., Mendes, J., Moreira, M., Grunenwald, T. (1999), “A Theoretical Model for Nonlinear Planar Motions of Rotors Under Fluid Confinement”, Journal of Fluids and Structures, Vol. 13, pp. 3-21.

Antunes, J., Piteau, P. (2001), “A Nonlinear Model for Squeeze-Film Dynamics Under Axial Flow”, ASME Pressure Vessel and Piping Conference – Symposium on Flow-Induced Vibration, Atlanta, July 2001, USA.

Antunes, J., Piteau, P. (2010), “A Nonlinear Analytical Model for the Squeeze-Film Dynamics of Parallel Plates Subjected to Axial Flow”, International Journal of Mechanical Sciences, in print.

Axisa, F., Antunes, J. (1992), “Flexural Vibrations of Rotors Immersed in Dense Fluids: Part 1 - Theory”, Journal of Fluids and Structures, Vol. 6, pp. 3-21.

Blevins, R. (1984), “Fluid Dynamics”, Van Nostrand Reinhold Company, New York, USA.

Childs, D. (1993), “Turbomachinery Rotordynamics: Phenomena, Modeling and Analysis”, John Wiley & Sons, New York, USA.

Esmonde, H., Fitzpatrick, J., Rice, H., Axisa, F. (1990a), “Analysis of Nonlinear Squeeze-Film Dynamics: I-Physical Theory and Modeling”, ASME Pressure Vessel and Piping Conference, Nashville, June 1990, USA.

Esmonde, H., Axisa, F., Fitzpatrick, J., Rice, H. (1990b), “Analysis of Nonlinear Squeeze-Film Dynamics: II-Experimental Measurement and Model Verification”, ASME Pressure Vessel and Piping Conference, June 1990, Nashville, USA.

Fritz, R. (1970), “The Effects of an Annular Fluid on the Vibrations of a Long Rotor: Part 1 - Theory”, ASME Journal of Basic Engineering, Vol. 92, pp. 923-929.

Grunenwald, T. (1994), “Comportement Vibratoire d’Arbres de Machines Tournantes dans un Espace Annulaire de Fluide de Confinement Modéré”, Doctoral Thesis, Paris University, September 1994.

Hirs, G. (1973), “A Bulk-Flow Theory for Turbulence in Lubricant Films”, ASME Journal of Lubrication Technology, Vol. 95, pp. 137-146.

Hobson, D. E. (1982) “Fluid-Elastic Instabilities Caused by Flow in an Annulus”, Proceedings of the 3rd International Conference on Vibration in Nuclear Plant, Keswick, UK, pp. 440-463 (BNES, London).

Idel'Cik, I. (1960), “Memento des Pertes de Charge”, Editions Eyrolles, Paris, France. Also published in 1994 as “Handbook of Hydraulic Resistance”, CRC Press, Boca Raton, USA.

Inada, F., Hayama, S. (1990a), “A Study of Leakage-Flow-Induced Vibrations: Part 1 – Fluid Dynamic Forces and Moments Acting on the Walls of a Narrow Tapered Passage. Journal of Fluids and Structures, Vol. 4, pp. 395-412.

Inada, F., Hayama, S. (1990b), “A Study of Leakage-Flow-Induced Vibrations: Part 2 – Stability Analysis and Experiments for Two-Degree-of-Freedom Systems Combining Translational and Rotational Motions. Journal of Fluids and Structures, Vol. 4, pp. 413-428.

Kaneko, S., Nakamura, T., Inada, F., Kato, M. (2008) “Flow Induced Vibrations: Classifications and Lessons from Practical Experiences”, Elsevier, Amsterdam, The Netherlands.

Moreira, M., Antunes, J., Pina, H. (2000a), “An Improved Linear Model for Rotors Subjected to Dissipative Annular Flows”, Proceedings of the 7th International Conference on Flow-Induced Vibration (FIV2000), June 2000, Lucerne, Switzerland.

Moreira, M., Antunes, J., Pina, H. (2000b), “A Theoretical Model for Nonlinear Orbital Motions of Rotors under Fluid Confinement”, Journal of Fluids and Structures, Vol. 14, pp. 635-668.

Mulcahy, T. M. (1980), “Fluid Forces on Rods Vibrating in a Finite Length Annular Region”, ASME Journal of Applied Mechanics, Vol. 47, pp. 234-240.

Mulcahy, T. M. (1988), “One-Dimensional Leakage-Flow Vibration Instabilities”, Journal of Fluids and Structures, Vol. 2, pp. 383-403.

Païdoussis, M. P. (1998), “Fluid-Structure Interactions: Slender Structures and Axial Flow – Vol. 1”, Academic Press, San Diego, USA.

Piteau, P., Antunes, J. (2010), “A Theoretical Model and Experiments on the Nonlinear Dynamics of Parallel Plates Subjected to Laminar/Turbulent Squeeze-Film Forces”, submitted for publication in Journal of Fluids and Structures.

Porcher, G., DeLangre, E. (1997), “A Friction-Based Model for Fluidelastic Forces Induced by Axial Flow”, Proceedings of the 4th International Symposium on Fluid-Structure Interaction, November 1997, Dallas, USA.